

# Designing an all-optical biosensor using photonic crystal

MAHSA BAZARGANI, BEHNAZ GHAREKHANLOU\*, MEHDI BANIHASHEMI

*Department of Electrical Engineering, Central Tehran Branch, Islamic Azad University, Tehran, Iran*

In this paper, we designed a small-size biosensor to detect the DNA molecules using a 2D hexagonal photonic crystal without any change in the radius of the holes. The sensing mechanism is based on the change in the refractive index of sensing holes and the intensity variation of the output transmission spectrum. By infiltrating the analyte within the sensing holes for one unit change in the refractive index, the normalized intensity of the transmission spectrum is reduced to 4 units. To analyze the performance of this structure, we used the plane wave expansion and the finite difference time domain methods. The regression coefficient is equal to -0.9689.

(Received July 28, 2020; accepted June 7, 2022)

*Keywords:* Biosensor, Photonic crystal, Resonant cavities, Intensity variation

## 1. Introduction

Photonic crystals (PCs) are one of the best items to guide and control photons [1,2]. The materials of these structures are composed of periodic layers with different refractive indexes in one, two, or three dimensions. The result of this periodic lattice is a photonic bandgap (PBG), a certain range of wavelengths that cannot be entered into the structure [3,4]. This region depends on various parameters such as lattice constant, the radius of components (dielectric rods or air holes in slab), and the dielectric constant of materials. We can create point or line defects to break the band gap and confine or guide the photons through it [5,6]. Designing various components depends on the type of defects in the structure. Therefore, the shape of the defect is important, and many interesting optical elements can be designed by creating different defects in the structure, such as optical logic gates [7], modulators [8], power splitters [9], optical filters [10], optical demultiplexers [11], optical polarization splitters [12], optical flip-flops [13], optical adders [14], and optical sensors. So far, various optical sensors have been presented using photonic crystals; one of them is a biosensor for detecting biological molecules, bacterial cells, viruses, proteins, DNA molecules, etc. [15-17]. The identification method in biosensors is based on infiltrating the analytes into the sensing holes and changing the refractive index. Generally, there are two mechanisms to study the sensor performance, the first method is based on the amount of resonant wavelength shift (RWS), and the second method is based on the intensity variation (IV) of the output transmission spectrum [18]. In the RWS method to detect the features of analytes, the amount of resonant wavelength shift is measured, and due to changes in the refractive index of the sensing area, the widespread displacement of wavelength is desirable. The RWS is favorable in a wide range of changes in the refractive index but often cannot be used to detect tiny changes in the refractive index. However, the IV method is used for

small refractive index changes with high accuracy, and often it is not desirable to measure wide changes of wavelength to improve the sensitivity. The important parameter to determine the accuracy of biosensors is sensitivity. In the RWS method, the sensitivity is the amount of change in resonant wavelength per refractive index unit. On the other hand, the sensitivity in the IV method is the amount of change in intensity per refractive index unit [19]. In this work, we present a photonic crystal biosensor by using resonant cavities. To calculate the photonic bandgap, we used the plane wave expansion (PWE) method [20]. Moreover, to study the optical properties of the structure, we used the finite difference time domain (FDTD) method [21].

## 2. Design and simulation

Our structure is based on a 2D hexagonal lattice of air holes in a dielectric slab. The number of holes in the x-direction is 30 and in the z-direction is 15. The lattice constant of structure and radius of air holes is 220 nm and 88 nm, respectively, and the effective refractive index of the slab is equal to 2.8. The contour map of the index profile of the structure before introducing the defects is shown in Fig. 1. The dispersion diagram of the structure should be obtained to find the operating wavelength. In Fig. 2, the band structure diagram is plotted along the edges of the irreducible Brillouin zone ( $\Gamma$ , M, and K are the three corners of the irreducible Brillouin zone). Two photonic band gaps can be seen; the transverse electric (TE) mode in  $0.3 \leq a/\lambda \leq 0.45$  range and the transverse magnetic (TM) mode in  $0.8 \leq a/\lambda \leq 0.84$  range. By choosing the range of TE mode for all the simulations in this design, the PBG will be in the  $488 \leq \lambda \leq 733$  (nm) wavelength range. In our design, the schematic of the structure consists of resonant cavities, sensing holes, and two waveguides as input and output. To couple the light at the input of structure, we used a temporal pulse source, and

for obtaining the output transmission spectrum, a time monitor is used at the output waveguide. To find the best sensing hole, we checked a large number of holes. Since changing the refractive index of holes far away from the cavity does not significantly affect the intensity of the output spectrum, we just brought the results of changing the refractive index in the four rows near the cavity. We changed the refractive index from 1.33 to 1.45 for each hole (the refractive index of holes containing water molecules and DNA molecules is 1.33 and 1.45, respectively). The schematic of the structure is shown in Fig. 3, and the results are given in Table 1 (We numbered the holes from left to right).

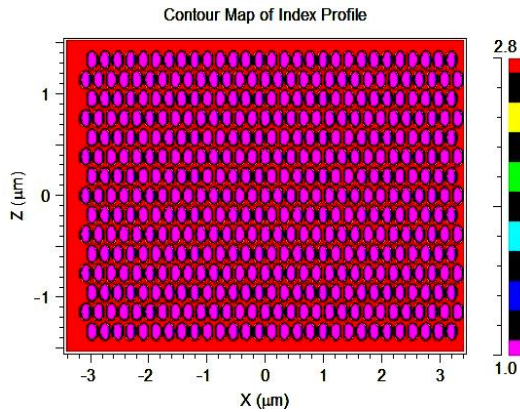


Fig. 1. The contour map of index profile (color online)

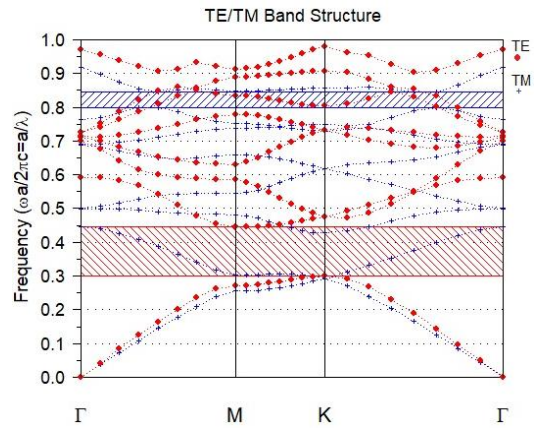


Fig. 2. The band structure of diagram (color online)

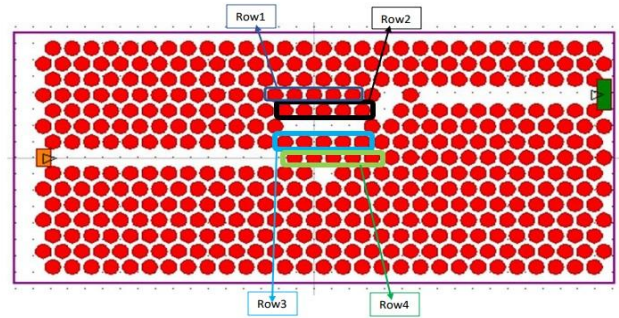


Fig. 3. Schematic of structure (color online)

Table 1. The results of changing the refractive index of the holes from row 1 to row 4

|      | hole | Binding water           |                                    | Binding DNA             |                                    |
|------|------|-------------------------|------------------------------------|-------------------------|------------------------------------|
|      |      | Central wavelength (nm) | Normalized Intensity of the output | Central wavelength (nm) | Normalized Intensity of the output |
|      | H1   | 644.8                   | 0.468                              | 644.8                   | 0.531                              |
|      | H2   | 644.8                   | 0.5                                | 644.8                   | 0.562                              |
| Row1 | H3   | 644.8                   | 0.781                              | 645.2                   | 0.562                              |
|      | H4   | 644.8                   | 0.593                              | 645.2                   | 0.625                              |
|      | H5   | 644.8                   | 0.912                              | 644.8                   | 0.862                              |
|      | H1   | 645.1                   | 0.656                              | 645.1                   | 0.593                              |
|      | H2   | 645.1                   | 0.781                              | 645.5                   | 0.531                              |
| Row2 | H3   | 646.2                   | 0.75                               | 646.5                   | 0.562                              |
|      | H4   | 645.5                   | 0.781                              | 645.6                   | 0.656                              |
|      | H5   | 645.15                  | 0.668                              | 645.15                  | 0.656                              |
|      | H1   | 645.15                  | 0.912                              | 645.15                  | 0.668                              |
|      | H2   | 645.2                   | 0.75                               | 645.5                   | 0.981                              |
| Row3 | H3   | 645.8                   | 0.981                              | 646.2                   | 0.8                                |
|      | H4   | 645.6                   | 0.412                              | 645.5                   | 0.75                               |
|      | H5   | 645.65                  | 0.812                              | 645.65                  | 0.656                              |
|      | H1   | 644.8                   | 1                                  | 645.6                   | 0.843                              |
|      | H2   | 645.4                   | 0.23                               | 645.5                   | 0.375                              |
| Row4 | H3   | 645.15                  | 0.875                              | 645.15                  | 0.812                              |
|      | H4   | 644.8                   | 0.906                              | 644.8                   | 0.843                              |
|      | H5   | 644.8                   | 0.562                              | 644.8                   | 0.656                              |

In the IV method, the central wavelengths of both spectrums must have the same value. According to Table 1, it seems that the fifth hole from row 1, the first and fifth holes from row 3, and the third and fourth holes from row 4 (which have the highest value of intensity) are more suitable as sensing holes. Then to increase the interaction of light and analyte to improve the identification accuracy, we infiltrated the analyte into the H6 hole, too (after checking many holes). We compared the results of infiltration into each one of the selected holes with simultaneous infiltration of H6, respectively (shown in Fig. 4 to Fig. 8). As mentioned earlier, according to Mechanism IV, the amount of change in the intensity of the output spectrum is important for us. Therefore, according to Table 2 and comparing the figures, we choose Fig. 7 as the best structure.

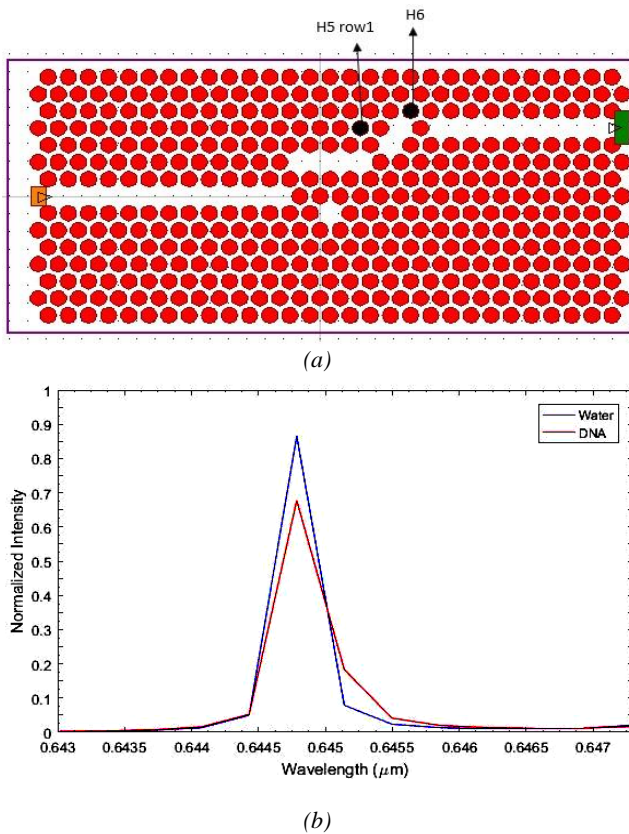


Fig. 4. (a) The schematic of structure (b) the normalized intensity outputs after binding the analytes into the H5 from row1 and H6 holes (color online)

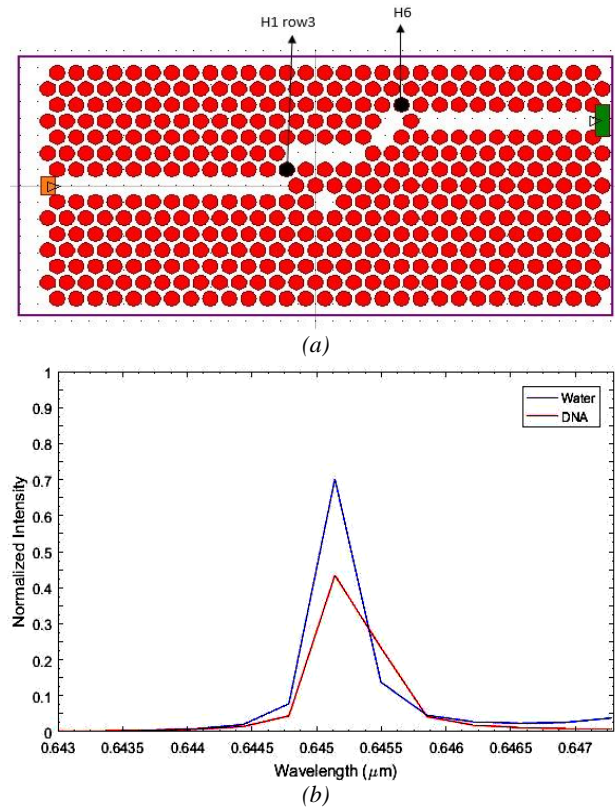


Fig. 5. (a) The schematic of structure (b) the normalized intensity outputs after binding the analytes into the H1 from row3 and H6 holes (color online)

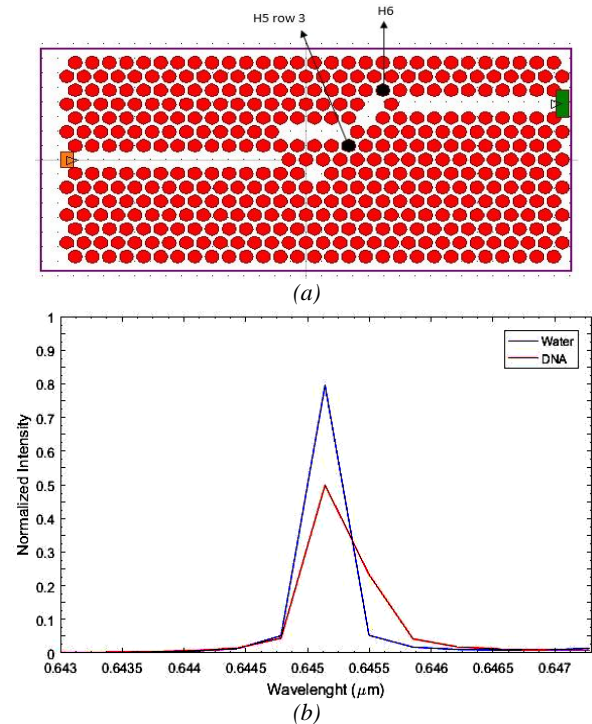


Fig. 6. (a) The schematic of structure (b) the normalized intensity outputs after binding the analytes into the H5 from row3 and H6 holes (color online)

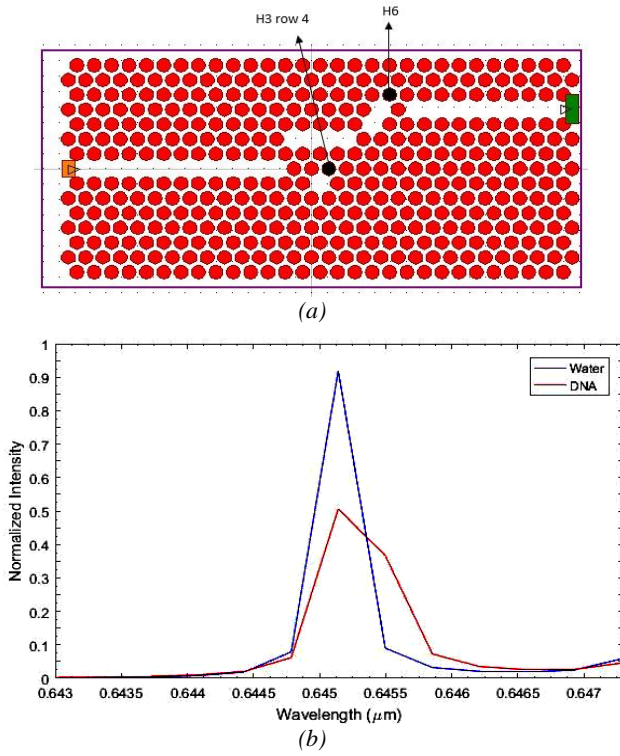


Fig. 7. (a) The schematic of structure (b) the normalized intensity outputs after binding the analytes into the H3 from row4 and H6 holes (color online)

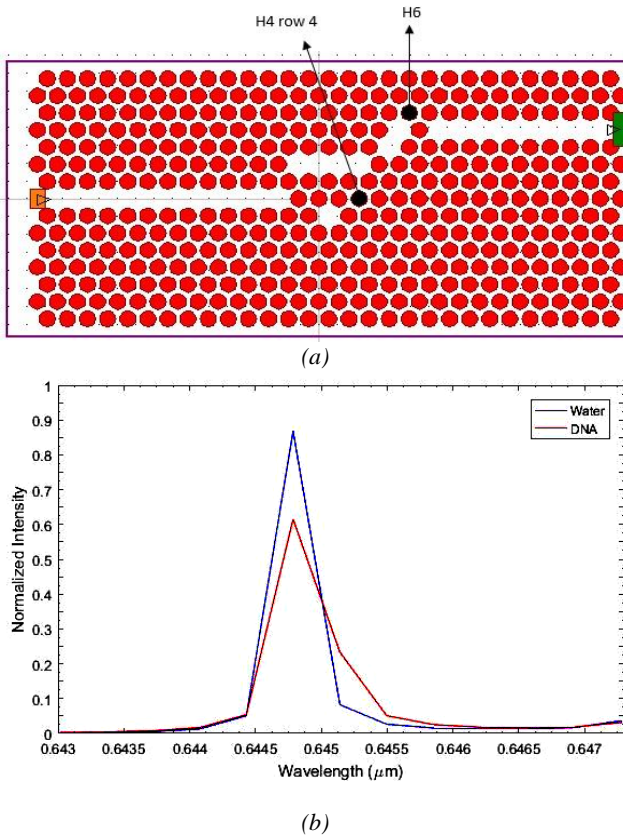


Fig. 8. (a) The schematic of structure (b) the normalized intensity outputs after binding the analytes into the H4 from row4 and H6 holes (color online)

Table 2. The normalized intensity by changing the refractive index holes from 1.33 to 1.45

| Sensing holes       | Normalized Intensity for n=1.33 | Normalized Intensity for n=1.45 | $\Delta I$ for $\Delta n = 1.2$ unit |
|---------------------|---------------------------------|---------------------------------|--------------------------------------|
| H5 from row1 and H6 | 0.86                            | 0.675                           | 1.85 unit                            |
| H1 from row3 and H6 | 0.7                             | 0.428                           | 2.72 unit                            |
| H5 from row3 and H6 | 0.872                           | 0.51                            | 3.62 unit                            |
| H3 from row4 and H6 | 0.915                           | 0.5                             | 4.15 units                           |
| H4 from row4 and H6 | 0.87                            | 0.61                            | 2.6 unit                             |

We increased the refractive index by 0.01 steps to observe the sensor's accuracy. The results are shown in Fig. 9. The quality factor (Q) is the ratio of the resonance wavelength ( $\lambda_{\max}$ ) and the full width half maximum (FWHM). That is calculated from Equation 1 and is brought in Fig. 10.

$$Q = \frac{\lambda_{\max}}{FWHM} \quad (1)$$

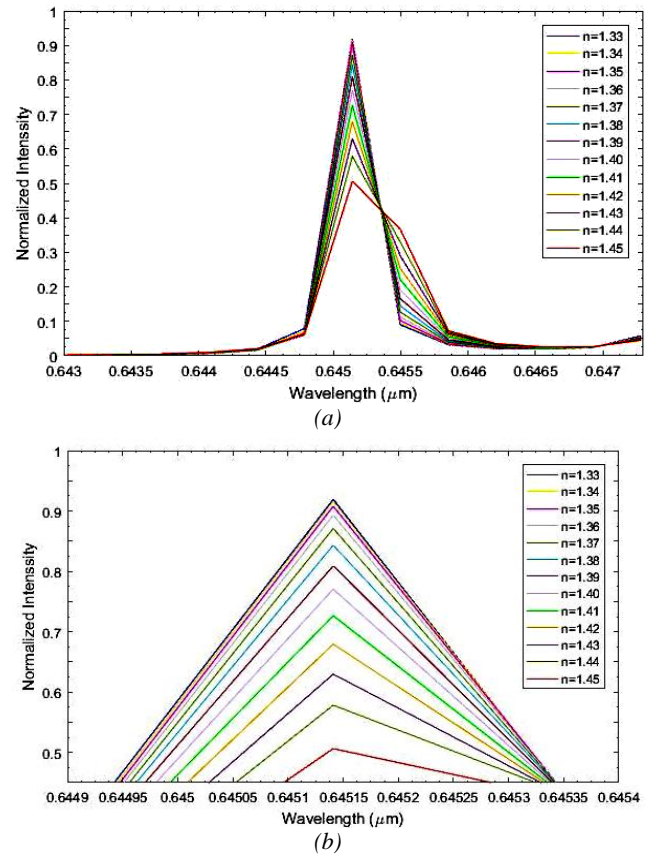


Fig. 9. The output normalized intensity of structure by increasing the refractive index of sensing holes from 1.33 to 1.45 by 0.01 steps. (b) the output normalized intensity in more details (color online)

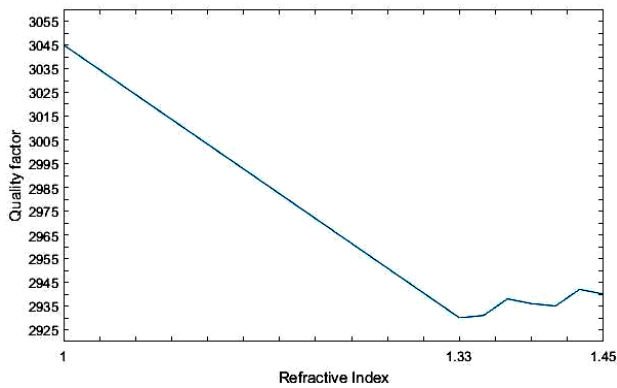


Fig. 10. The quality factor of structure by considering H3 from row4 and H6 as sensing holes (color online)

### 3. Results and discussion

In this work, to simulate and investigate the behavior of optical wave propagation, the 2D finite difference time domain (FDTD) method was used based on the effective refractive index, and the IV mechanism was used to sense the DNA molecules. Many holes have been checked for infiltration to find the best sensing area. The H3 hole from row4 with the H6 hole was selected as the sensing hole according to simulation results. To observe the sensor's accuracy, we increased the effective refractive index of sensing holes from 1.33 to 1.45 by 0.01 steps in 13 levels. The normalized curves of the intensity shift according to the change in refractive index are shown in Fig. 11. If the refractive index of sensing holes is 1.33, the shift of intensity is zero. By increasing the refractive index, the intensity of the output spectrum is shifted to lower values. The regression coefficient is equal to -0.9689, which shows an approximately linear relationship between them.

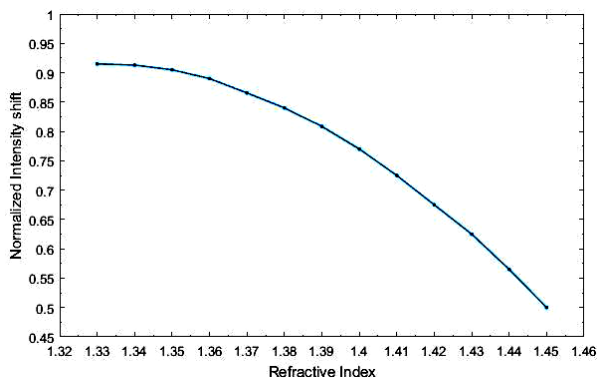


Fig. 11. The normalized intensity shifts of the resonant wavelength in relation to the refractive index in sensing holes (color online)

### 4. Conclusion

In this paper, to identify the target molecule based on the IV method without any change in the size of the holes' radius, the intensity of the output spectrum was measured, and it was compared with the results of water infiltration. If the infiltrated analyte is DNA, the output intensity in resonant wavelength decreases. According to the IV

method to calculate the sensitivity of this sensor, the amount of change in the intensity of the transmission spectrum per unit of refractive index change was measured, which was four units. So, for changing the refractive index of the sensing holes from 1.33 to 1.45 (that is 1.2 units), the amount of change in the intensity of the transmission spectrum was calculated, which was equal to 4.15 units. And the regression coefficient was -0.9689.

### References

- [1] G. H. Delphi, S. Olyae, M. Seifouri, A. Mohebzadeh Bahabady, *Photonic Netw. Commun.* **38**(2), 250 (2019).
- [2] K. Venkatachalam, D. S. Kumar, S. Robinson, *Photon. Netw. Commun.* **34**(1), 100 (2017).
- [3] A. Tavousi, M. Mansouri-Birjandi, *Photonic Netw. Commun.* **32**(1), 160 (2016).
- [4] F. Mehdizadeh, M. Soroosh, *Photon. Netw. Commun.* **31**(1), 65 (2015).
- [5] H. Alipour Banaei, F. Mehdizadeh, B. Amini, *IJFCC* **4**(4), 346 (2015).
- [6] M. Seifouri, V. Fallahi, S. Olyae, *Photon. Netw. Commun.* **35**(2), 225 (2018).
- [7] A. Mohebzadeh Bahabady, S. Olyae, *IET Optoelectron.* **12**(4), 191 (2018).
- [8] D. J. Thomson, F. Y. Gardes, Y. Hu, G. Mashanovich, M. Fournier, P. Grosse, J-M. Fedeli, G. T. Reed et al., *Opt. Express* **19**(12), 11507 (2011).
- [9] A. Ghaffari, F. Monifi, M. Djavid, M. S. Abrishamian, *J. Appl. Sci.* **8**(8), 1416 (2008).
- [10] S. Naghizade, S. M. Sattari-Esfahlan, *J. Opt. Commun.* **40**(1), 1 (2017).
- [11] S. Naghizade, S. M. Sattari-Esfahlan, *J. Opt. Commun.* **41**(1), 1 (2018).
- [12] T. Liu, A. R. Zakharian, M. Fallahi, J. V. Moloney, M. Mansuripur, *IEEE Photonics Technol. Lett.* **17**(7), 1435 (2005).
- [13] S. S. Zamanian-Dehkordi, M. Soroosh, G. Akbarizadeh, *Optical Review* **25**, 523 (2018).
- [14] M. J. Maleki, A. Mir, M. Soroosh, *Opt. Quant. Electron.* **52**(196), 3 (2020).
- [15] S. Olyae, A. Mohebzadeh Bahabady, *Optik* **126**(20), 2560 (2015).
- [16] H. Mohsenirad, S. Olyae, M. Seifouri, *Photon Lasers Med.* **5**(1), 51 (2015).
- [17] S. Robinson, N. Dhanlaxmi, *Photonic Sens.* **7**(1), 11 (2017).
- [18] C. Y. Chao, L. J. Guo, *J. Lightwave Technol.* **24**(3), 1395 (2006).
- [19] S. Olyae, A. Mohebzadeh-Bahabady, *Opt. Quant. Electron.* **47**, 1881 (2014).
- [20] S. G. Johnson, J. D. Joannopoulos, *Opt. Express* **8**(3), 173 (2001).
- [21] A. Taflove, S. C. Hagness, *Computational Electrodynamics: The Finite Difference Time Domain Method*, 3th ed., rev., Artech House, London (UK), (2005).

\*Corresponding author: gharekhanlou@iauctb.ac.ir